10-27-2011

Multiregime states of Arctic atmospheric circulation

B. J. Fisel
Iowa State University, bjfisel@gmail.com

W. J. Gutowski Jr.
Iowa State University, gutowski@iastate.edu

J. M. Hobbs
Iowa State University, hobbs.jonathan.m@gmail.com

J. J. Cassano
Iowa State University

Multiregime states of Arctic atmospheric circulation

Abstract
[1] Ensemble simulations of Arctic circulation can develop multiple dynamical regimes. We use ensemble simulations for June–December 2007 by the Advanced Research Weather Research and Forecasting model to examine regime development and to understand differences in the atmospheric circulation regimes caused by sea ice. Multiple regimes are common in our ensemble simulations, although there are differences through the period. Multiple-regime states tend to be preferred slightly more in June, July, and August than October, November, and December. September has the fewest multiple-regime periods. September is also the month of sea ice minimum, suggesting that open ocean may inhibit the occurrence of multiple regimes in ensemble simulations compared to periods when substantial sea ice is present. The regime behavior occurring here suggests that as future summer ice cover wanes in the Arctic, the predictability of the atmosphere may increase.

Keywords
Arctic atmospheric circulation, Multiple circulation regimes

Disciplines
Climate

Comments
This article is from *Journal of Geophysical Research: Atmospheres* 116 (2011): D20122, doi:10.1029/2011JD015790. Posted with permission.

Multiregime states of Arctic atmospheric circulation

B. J. Fisel,[1] W. J. Gutowski Jr.,[2] J. M. Hobbs,[1] and J. J. Cassano[2]

Received 8 February 2011; revised 19 August 2011; accepted 30 August 2011; published 26 October 2011.

[1] Ensemble simulations of Arctic circulation can develop multiple dynamical regimes. We use ensemble simulations for June–December 2007 by the Advanced Research Weather Research and Forecasting model to examine regime development and to understand differences in the atmospheric circulation regimes caused by sea ice. Multiple regimes are common in our ensemble simulations, although there are differences through the period. Multiple-regime states tend to be preferred slightly more in June, July, and August than October, November, and December. September has the fewest multiple-regime periods. September is also the month of sea ice minimum, suggesting that open ocean may inhibit the occurrence of multiple regimes in ensemble simulations compared to periods when substantial sea ice is present. The regime behavior occurring here suggests that as future summer ice cover wanes in the Arctic, the predictability of the atmosphere may increase.

Citation: Fisel, B. J., W. J. Gutowski Jr., J. M. Hobbs, and J. J. Cassano (2011), Multiregime states of Arctic atmospheric circulation, *J. Geophys. Res.*, *116*, D20122, doi:10.1029/2011JD015790.

1. Introduction

[2] Previous work has shown that Arctic atmospheric circulation responds to changes in forcing as a dynamical system, wherein the response is not a simple cause and effect relationship, but rather a change in circulation patterns [*Gutowski et al.*, 2007]. An example where surface conditions can change forcing is through the behavior of Arctic sea ice, which acts to regulate the strength of energy fluxes linking the ocean and atmosphere. In this study, we examine the effects of sea ice on the development of circulation regimes in the western Arctic Ocean. In the last decade, multiyear Arctic sea ice has declined rapidly [*Comiso*, 2006], a behavior attributed to natural and anthropogenic causes [*Serreze et al.*, 2007]. Climate models participating in the Intergovernmental Panel on Climate Change Fourth Assessment Report (IPCC AR4) are in agreement with the recent decline in Arctic sea ice cover [*Zhang and Walsh*, 2006], although observations show sea ice declining faster than simulated [*Stroeve et al.*, 2007]. During the summer of 2007, a record minimum occurred in Arctic sea ice area, which raised concerns regarding further long-term decline in Arctic sea ice [*Comiso et al.*, 2008]. *Comiso et al.* [2008] attributed the loss of Arctic sea ice to the ice-albedo feedback, whereby increases in summer open ocean allows more solar radiation to be absorbed, delaying the refreezing of sea ice, thereby creating thinner seasonal sea ice, leading to greater absorption of energy, which promotes further reductions to summer sea ice.

[3] Various observational studies have investigated the decline of Arctic sea ice and its effect on the atmospheric circulation. *Walsh and Johnson* [1979] found an anomalous warming of the polar atmosphere during periods of reduced ice concentrations north of 60°N. Later, *Alexander et al.* [2004] found large anomalies in surface air temperatures and air-sea heat fluxes during two winters with reduced ice concentrations in the Greenland Sea. Similarly, *Slonosky et al.* [1997] found decreased 500 hPa heights and mean sea level pressure (MSLP) in the Greenland Sea with reduced sea ice concentrations. Other studies suggested that reductions in sea ice produce substantially larger energy exchanges between the ocean and atmosphere [*Walsh*, 1983; *Honda et al.*, 1996; *Francis et al.*, 2009].

[4] Recent modeling studies have also examined the atmospheric response to specified changes in sea ice area. Using the Goddard Institute for Space Studies global climate model, *Parkinson et al.* [2001] found that specifying reduced (increased) sea ice area yielded increased (decreased) Arctic surface air temperatures. *Deser et al.* [2004] investigated the wintertime atmospheric response to sea ice trends using the Community Climate Model, Version 3.0 (CCM 3.0). They found a shallow, anomalous atmospheric ridge in the Greenland Sea that developed in areas of reduced ice cover in response to heating that large static stability confined to the lower troposphere. In a similar study, *Alexander et al.* [2004] also found for areas of reduced ice cover a local but shallow response in surface air temperatures and decreases in sea level pressure. Additionally, they noted that ice anomalies occurring along storm tracks in the Greenland Sea may affect the low-level baroclinicity, allowing for shifts in storm tracks. *Bhatt et al.* [2008], using CCM 3.6, investigated the atmospheric response in the Arctic during a period with small sea ice area, for the months April–October 1995. The largest response occurred in August when the Arctic sea ice area was near its minimum. During this period, the Arctic displayed a shallow temperature response with small

[1]Department of Geological and Atmospheric Sciences, Iowa State University, Ames, Iowa, USA.
[2]Department of Geological and Atmospheric Sciences, Iowa State University, Ames, Iowa, USA.

0148-0227/11/2011JD015790

decreases in sea level pressure. One further experiment limited ice reduction to only the Beaufort Sea, in which they found a similar but smaller response. Additionally, they found sea ice anomalies to have an influence on the storm tracks in the North Pacific region. *Singarayer et al.* [2006] examined the impacts of a 21st century, reduced sea ice scenario using the Hadley Centre Atmospheric Model, Version 3 (HaDAM3). The impact was stronger in winter with warming over the Arctic basin and reductions in sea level pressure extending into the North Pacific and North Atlantic regions. *Higgins and Cassano* [2009] examined the influence of projected late 21st century reductions of sea ice on atmospheric circulation and found changes across the Arctic resulting from changes in the frequency of high and low pressure centers and overall deepening of the Aleutian Low. *Strey et al.* [2010] simulated the effects of reduced sea ice in 2007 compared to the 1984 distribution for the period September–December 2007 and found significant atmospheric differences resulting from the changed ice distribution in October. Finally, using a general circulation model, *Petoukhov and Semenov* [2010] found that anomalously low sea ice in the Barents and Kara seas could yield extremely cold winters over Europe.

[5] In this study we describe another influence sea ice cover has on Arctic atmospheric circulation, namely the emergence of multiple dynamic circulation regimes in ensemble simulations. In this context, we view the atmosphere as a dynamic system in which different realizations may at times follow different circulation evolution [*Sivillo et al.*, 1997]. There is a tendency for MSLP to evolve differently among ensemble members, leading to a splitting into multiple dynamic regimes that appear to result from unforced, nonlinear variability. The development of multiple regimes implies that there is not a single circulation evolution that one might be able to forecast, thus implying reduced predictability of the flow. *Alexandru et al.* [2007] found apparent instances of multiple circulation regimes in their analysis of internal variability in North American regional climate simulations. However, their domains allowed lateral boundary conditions to govern the freedom of their ensemble to develop multiple regimes. In this study, the Arctic circumpolar vortex is generally contained within the domain, allowing the simulations to evolve without being strongly constrained by the lateral boundary conditions [*Gutowski et al.*, 2007]. In contrast to studies such as *Alexandru et al.* [2007] and *Lucas-Picher et al.* [2008], which describe unforced internal variability that appears as "noise" in regional climate simulations, here we describe statistically distinct regimes that appear in ensemble simulations of Arctic atmospheric circulation. We note that dynamic regimes discussed in this work are different from the orographically forced multiple equilibrium states found by *Charney and DeVore* [1979], and the bimodal distribution of wave states found by *Hansen* [1988].

2. Data and Methodology

2.1. Model Design

[6] For our ensemble simulations, we used the Weather Research and Forecast model: Advanced Research WRF (WRF-ARW), Version 3.1.0 [*Skamarock et al.*, 2008]. An important consideration for the WRF-ARW simulations was the selection of physical parameterizations appropriate to the Arctic. The ensemble simulations here used parameterization choices similar to *Cassano et al.* [2011] with some modification of these choices based on additional model testing and evaluation provided by M. Seefeldt (unpublished data, 2010). The chosen parameterizations include the subgrid cumulus scheme of *Grell and Devenyi* [2002], the NCAR Community Atmosphere Model (CAM 3.0) spectral band scheme [*Collins et al.*, 2004; *Mlawer et al.*, 1997] for shortwave and longwave radiation, and the Goddard Cumulus Ensemble (GCE) models [*Tao and Simpson*, 1993] cloud microphysics scheme using a three-category ice phase scheme, with the *Rutledge and Hobbs* [1984] graupel ice physics as the third class of ice. For the planetary boundary layer (PBL), we used the Mellor-Yamada-Janjic (MYJ) scheme [*Janjic*, 2001], which is based on eta surface similarity theory [*Monin and Obukhov*, 1954].

[7] We used the four-layer Noah [*Chen and Dudhia*, 2001] land surface model (LSM) with polar modifications for snow and ice [*Hines et al.*, 2011]. Updates include the representation of sea ice as a fractional field in a grid box. For specified sea ice concentrations, surface layer routines determine the ice surface temperature from the energy exchanges between the atmosphere and underlying ocean. Additionally, the model set sea ice thickness at 3 m and sea ice albedo and emissivity at 0.80 and 0.98, respectively. In the work here, we treat sea ice using two different methods: one set of simulations allows an ocean grid box in selected locations (see section 2.3) to have ice cover anywhere in the range 0–100% (fractional), and the other set of simulations specifies sea ice cover as either 0% or 100% in a grid box (binary).

[8] The simulations used 40 terrain-following vertical levels between the Earth's surface and the model top at 50 hPa. In order to resolve the boundary layer well, the model used 10 levels between the surface and 800 m. The model domain (Figure 1) is a polar-stereographic projection of the Arctic specified by the Coordinated Regional Downscaling Experiment (CORDEX) (unpublished data, 2010) available from the World Climate Research Program (http://wcrp.ipsl.jussieu.fr/SF_RCD_CORDEX.html). The domain is spanned by a 126 × 136 array of grid points with 50 km grid spacing, centered over the Arctic Ocean and covering portions of the Arctic North America and Eurasia.

2.2. Data

[9] The ensemble simulations used initial and lateral boundary conditions for atmospheric fields provided by the European Centre for Medium-Range Forecasts Interim Re-analysis (ERA-Interim), available every 6 h at T255 (approximately 0.7°) horizontal resolution [*Simmons et al.*, 2007; *Berrisford et al.*, 2009]. The ERA-Interim also provided sea surface temperatures every 12 h with temperatures prescribed at the freezing point of salt water for sea ice concentrations equal to 100%. We also used the ERA-Interim to assess the quality of our ensemble simulations. Although the same data are supplying lateral boundary conditions, for a Pan-Arctic domain that encompasses most of the circumpolar vortex, the lateral boundary conditions exert relatively small influence on the model's interior circulation [*Gutowski et al.*, 2007]. This is in contrast to regional simulations in the midlatitudes, where westerly flow sweeps across the entire domain [*Giorgi and Bi*, 2000].

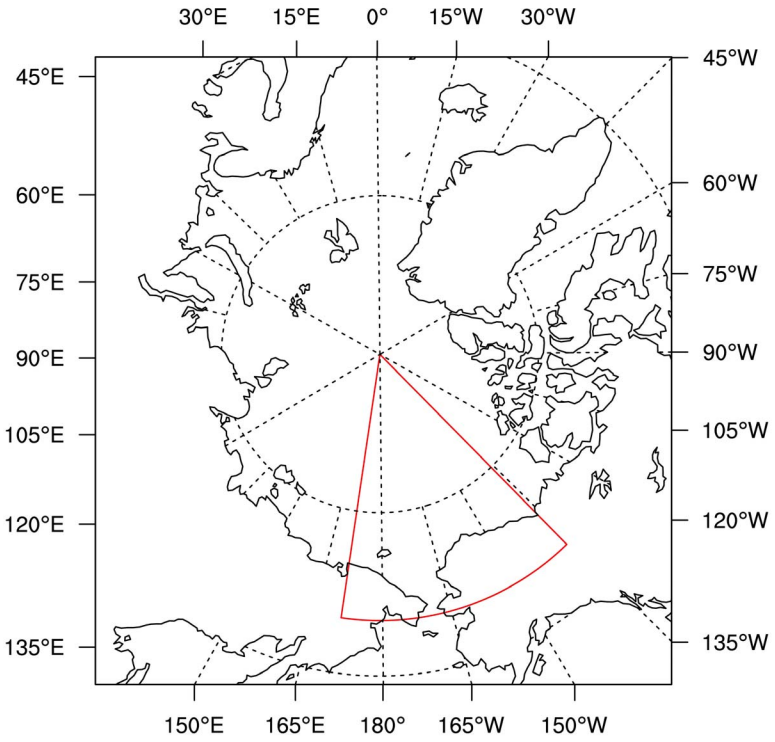

Figure 1. Map of the WRF model domain showing the land-sea mask at the model's 50 km resolution. Sea ice in the red triangle was subject to fractional sea ice treatment in some of the simulations. It is also the region used for diagnosing circulation regime behavior.

[10] We prescribe fractional sea ice using daily sea ice concentrations from the National Snow and Ice Data Center (NSIDC) Special Sensor Microwave/Imager (SSM/I) observations, available every 12 h at 25 km resolution [*Comiso*, 2008]. In the Arctic, sea ice concentrations are not available poleward of 87.2°N, so we assume a concentration there of 100%. Additionally, to account for potential errors associated with data retrieval and summer melt ponding [*Comiso and Kwok*, 1996; *Comiso et al.*, 1997], we follow the recommendation of *Comiso and Parkinson* [2008] and set ice concentrations of 10% or less to open ocean (0% ice cover). The WRF-ARW Preprocessing System (WPS) interpolates the sea ice concentrations on the NSIDC grid to values for each grid box in our ensemble simulations. For ensemble simulations with binary sea ice, we then adjust the sea ice fraction to 100% for grid boxes with NSIDC ice cover greater than or equal to 50%, and to 0% for grid boxes with NSIDC ice cover less than 50%.

2.3. Simulations

[11] The original intent of this study was to discern differences in atmospheric circulation due to binary or fractional treatment of sea ice. However, we found that the differences in these simulations are governed only weakly by the choice of ice treatment, and that a more important factor is the susceptibility of Arctic atmospheric circulation to developing multiple dynamic regimes. In line with our original intent, we constructed an ensemble with 16 members: 8 used binary sea ice everywhere and 8 used binary sea ice everywhere except for a portion of the Arctic Ocean that had fractional sea ice coverage in its grid boxes. The portion of the Arctic Ocean with prescribed fractional ice cover is an area north of 70°N that includes portions of the Arctic, Beaufort and Chukchi (ABCH) seas (Figure 1). As part of our original intent, we chose the ABCH seas region as the focus of our analysis because this region had a relatively large area of fractional ice cover between 50% and 90%. Under the binary ice treatment, grid boxes with observed ice fraction greater than 50% will have 100% ice cover, which reduces heat fluxes between the ocean and atmosphere, in contrast to the fractional treatment, which retains a portion of open ocean in these grid boxes, thus allowing potentially much greater heat fluxes between the ocean and atmosphere.

[12] Our ensemble of 16 members is comparable to ensemble sizes used by others studying uncertainty in extratropical circulation, for example, *Rinke and Dethloff* [2000] (4 members), *Alexandru et al.* [2007] (10–15 members), and *Lucas-Picher et al.* [2008] (10 members), although some have used larger ensembles, for example, *Wu et al.* [2005] (48 members). Perhaps more important, 16 members should be sufficient to obtain clear seasonal climate responses above noise levels [*Taschetto and England*, 2008]. The ensemble simulations ran from 00:00 UTC 24 May 2007 through 31 December 2007, with start times for each ensemble member staggered by 12 h during the period 24–30 May 2007 (Table 1). In viewing the atmosphere as a dynamic system, analysis began on 15 June, thereby allowing time for the ensemble simulations to lose memory of the initial conditions and provide different, independent realizations of atmospheric circulation by the start of the analysis period.

2.4. Regime Analysis

[13] Analysis of MSLP time series from our simulations, averaged over the analysis region in Figure 1, shows periods

Table 1. Ensemble Member Starting Times

Ensemble	Start Time
Fraction	
05/24	12Z
05/25	12Z
05/26	12Z
05/27	12Z
05/28	12Z
05/29	00Z
05/29	12Z
05/30	00Z
Binary	
05/25	00Z
05/26	00Z
05/27	00Z
05/28	00Z
05/28	12Z
05/29	00Z
05/29	12Z
05/30	00Z

when ensemble members collectively show two or more circulation regimes in our target region. We identify these regimes using model-based clustering, which is a common technique for systematically identifying combinations of similar components in multivariate data. For example, *Smyth et al.* [1999] use model-based clustering to identify multiple regimes in seasonal geopotential height anomaly patterns. A brief description of the regime analysis appears below, followed by a more in-depth description for those wishing more details. We discuss results of the analysis in section 3. The analysis follows these steps:

[14] 1. We use time windows (7 or 11 days) of time series of MSLP averaged over our analysis region to evaluate regimes, thus requiring circulation regimes to persist longer than the synoptic time scale.

[15] 2. We perform a cluster analysis on the MSLP time series based on mean values, trends and variability of MSLP for each ensemble member.

[16] 3. The Bayesian Information Criterion (BIC) parameter then provides a summary of model fit (e.g., one-regime model or two-regime model) that includes a penalty for model complexity.

[17] 4. The BIC determines whether single or multiple regimes are favored for each 7 day and 11 day time window.

[18] Model-based clustering characterizes the data as a finite-mixture stochastic model. A finite-mixture model assumes that the probability density function (PDF) for the data is a weighted average of a fixed set of $j = 1, 2, \ldots, k$ component PDFs f_j

$$f(y_{i,t}) = \sum_{j=1}^{k} w_j f_j(y_{i,t}|\theta_j). \tag{1}$$

[19] Here $y_{i,t}$ is the MSLP for ensemble member i at time t. Each component of the model in (1) is characterized by its own set of parameters θ_j and a weight w_j. For the ensemble MSLP time series, we assume that each ensemble member belongs to one of the k components, or regimes. However, the regime membership of each ensemble member, the regime weights and the regime-specific PDFs are unknown and need to be estimated from the data. This requires further assumptions about the nature of the individual PDFs.

[20] We adopt a time series stochastic model for the individual PDFs f_j. Specifically, if ensemble member i is in regime j, the observed time series follows a first-order autoregressive process

$$\begin{aligned} y_{i,t} &= \mu_{j,t} + \rho_j(y_{i,t-1} - \mu_{j,t-1}) + \varepsilon_{i,t}, \\ \varepsilon_{i,t} &\sim \text{Gaussian}\left(0, \sigma_j^2\right), \end{aligned} \tag{2}$$

with autocorrelation parameter ρ_j and Gaussian-distributed random shocks $\varepsilon_{i,t}$. Thus, each regime has its own autocorrelation parameter and variance. In addition, to allow the time series mean to vary with time, we add some flexibility to the mean parameters $\mu_{j,t}$. These are linear combinations of a set of B-spline basis functions, with the number of basis functions depending on the length of the time series. This allows the overall mean for each regime to vary smoothly with time, meaning that regimes could differ not only in their overall mean over the entire time series, but also in their trends over time. Regimes can also differ in their overall variability. For a given number of regimes, the data are used to identify the most likely parameter values for each regime and the most likely regime membership for each ensemble member.

2.4.1. Estimation

[21] For a specified number of regimes k, we estimate parameters by maximizing the likelihood function, denoted as $L(\theta|y)$ and the resulting estimates are known as the maximum likelihood estimates (MLE). The likelihood function is equivalent to the joint probability distribution for the data given the parameters. For a single regime and the Gaussian time series model in (2), the time series for a single ensemble member has a multivariate Gaussian joint distribution. In contrast, for multiple regimes, the joint distribution is a mixture of multivariate Gaussian distributions. For a mixture model such as (1), the expectation-maximization (EM) algorithm is a convenient tool for finding the MLE. The EM algorithm is an iterative search procedure that is designed to converge to the MLE and generally performs well in practice. *Raftery et al.* [2005] outline the general steps for each iteration of the algorithm for a mixture model with Gaussian component distributions. Once the parameter estimates that maximize the likelihood are found, one can also compute the most probable regime membership for the individual ensemble members.

2.4.2. Model Selection

[22] Maximum likelihood estimation also provides information about the relative quality of a model's fit to the data. One can compare competing statistical models by evaluating the likelihood function at the MLE for each model. However, a more complex model with more parameters will tend to provide a better fit, so a model comparison criterion should also incorporate model complexity. The Bayesian Information Criterion provides a summary of model fit that also includes a penalty for the number of parameters in the model. In the context of model-based clustering, *Fraley and Raftery* [2002] define

$$\text{BIC} = 2\ln(L(\theta_{MLE}|y)) - p\ln n, \tag{3}$$

where p is the number of model parameters, n is the sample size (the number of ensemble members), and $L(\theta_{MLE}|y)$ is the value of the likelihood function at the MLE. The BIC

Table 2. Performance Statistics of the Simulation Ensemble (ENS) Compared to ERA-Interim for the Whole Domain's MSLP (hPa)

Month	RMSD (ERA)	RMSD (ENS-ERA)	Bias (ENS-ERA)
June (15–30)	7.1	8.1	−0.8
July	5.8	6.7	0.3
August	6.4	8.2	2.0
September	5.6	8.3	−1.8
October	9.1	10.4	−1.0
November	9.5	12.1	−1.0
December	12.0	13.7	−0.5

can be used to compare the fit of mixture models for varying numbers of components. One primary comparison we make is a one-component mixture versus a two-component mixture. In the form of (3), a model with higher BIC is favored.

2.4.3. Time Windows

[23] We are interested in circulation regimes that persist beyond a synoptic time scale but wish to avoid examining long time series where transitions from one dynamic regime to another would be increasingly likely. Therefore, we perform the mixture model estimation on time series of MSLP that are 7 or 11 days long, with one observation per ensemble member per day. With 16 ensemble members present, there are generally sufficient data to estimate the mixture model parameters with precision for up to three regimes, while still including more than one ensemble member in a regime. The estimation is performed separately for every available 7 day and 11 day time window. Each time window is identified by its starting date. For example, the 7 day data set for 1 July consists of MSLP for 1–7 July and the 7 day data set for 31 July consists of MSLP for 31 July–6 August.

3. Results

3.1. Model Performance

[24] Using the ERA-Interim Re-analysis that supplied our initial and boundary conditions as our reference simulation, we calculated performance statistics (Table 2) to determine how well our ensemble simulations were reproducing Arctic atmospheric circulation. First, we computed the difference between the monthly, spatially averaged ensemble simulations, and the reanalysis. This was small (±2 hPa) for the months simulated. We were also interested in how our model ensemble simulations performed with respect to the noise level of natural variability. For each month, we computed at each grid point the mean squared difference in daily averaged MSLP time series between each ensemble member and the ERA-Interim Re-analysis. We averaged these squared differences over the simulation domain and over all ensemble members and then calculated the square root to obtain each month's root-mean-square difference (RMSD) in daily variability between the ensemble and the ERA-Interim. For comparison, we calculated the daily variability of the ERA-Interim Re-analysis by computing the square root of the variance between the daily averaged and monthly averaged MSLP. We use this daily variability as a metric for assessing the magnitude of the RMS differences between the ensemble and the reanalysis. Overall, the ensemble's RMSDs are similar to the ERA-Interim daily variability in MSLP. This result indicates that the ensemble's daily departures from the reanalysis are comparable to the observed daily variability. The RMSDs and biases in Table 2 thus indicate that the ensemble does not depart substantially from the observed behavior during the 6 month simulation.

3.2. Regime Behavior

[25] We diagnose regimes using time series of daily MSLP averaged over our analysis region in Figure 1. We highlight results that are common to both the 7 day and 11 day windows, to lessen dependence of our results on a specific window choice. Multiple regimes are common in our simulations, although there are differences in characteristics through the period. Multiple-regime behavior generally occurs in one of two ways (Figure 2): when daily MSLP traces show differing trends, whereby some ensemble members trend toward higher pressure and others trend toward lower pressure; and when MSLP traces become significantly separated, whereby some ensemble members have distinctly different MSLP versus other members. The regime behavior often occurs in sequence, with differing trends leading to separated pressure traces that then have differing trends as the traces merge into one regime later. Figure 3 shows examples of MSLP spatial distribution for each regime on 2 days when two regimes occurred in the ensemble. The MSLP shown is the average across all ensemble members in the same regime.

[26] Table 3 shows the percentage of days in each month when the BIC prefers two-regime or three-regime behavior over one-regime behavior. There is a slight tendency for two or three regimes to be preferred more in June-July-August (JJA) than in October-November-December (OND). However, the clearest feature in Table 3 is the September minimum, which coincides with the month that has the least amount of sea ice. Sea surface temperatures are specified in the ensemble simulations, which may act to constrain the atmospheric behavior [*Parkinson et al.*, 2001] and inhibit variability across ensemble members during periods when little sea ice is present. In contrast, ice surface temperature is computed internally by the model, so that when there is substantial sea ice area, the model potentially has more freedom to determine the evolution of surface skin temperature.

[27] We determined when variability across the ensemble was small during our simulations by computing for each day the interquartile difference (75th–25th quartiles) among the ensemble members for MSLP averaged over our analysis region and then averaging the interquartile difference over each month (Table 4). There is a wider range of variability occurring in OND (>8 hPa) than JJA and September (<8 hPa), which supports the concept that as sea ice area decreases, variability across the ensemble becomes small. Recalling that each regime is identified by its starting date, we have counted the number of consecutive days (streaks) that start multiple-regime behavior. These streaks (Table 5) are also important in recognizing periods when variability across the ensemble is small. Consecutive-day streaks are more persistent during JJA, which suggests that the model has a greater tendency to remain in one mode of regime behavior during JJA. Less frequent transitions between different modes of regime behavior suggests that the flow evolves more slowly in summer. In contrast, during periods with greater sea ice area in the model, the model-computed temperature for the ice surface appears to allow the model's

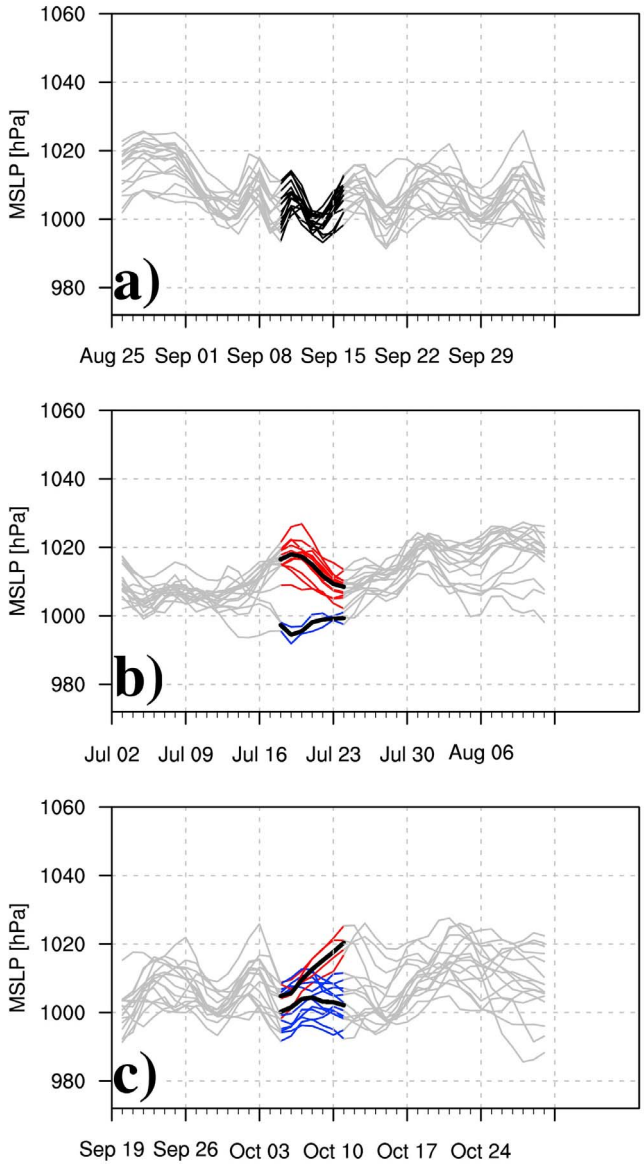

Figure 2. Time series of daily MSLP averaged over our analysis region showing episodes using a 7 day time window of (a) one regime, (b) two separated regimes, and (c) two regimes with different trends.

atmosphere to have more freedom in its variability and to transition more frequently between different regime modes.

[28] Recent studies examining seasonal cyclone variability have found differences in duration time and frequency of Arctic cyclones throughout the year [*Zhang et al.*, 2004; *Sorteberg and Walsh*, 2008; *Asplin et al.*, 2009]. During summer they found Arctic atmospheric circulation developed more persistent behavior with Arctic cyclones having a longer residence time than in colder months, which may have been the result of enhanced baroclinic instability when more open ocean was present. This is in line with our results that identified the JJA and September circulations as persisting longer. In contrast, in winter (i.e., periods with large sea ice area), Arctic cyclones were observed to be more frequent but have shorter duration times, which may be attributed to a reinforcement of anticyclonic circulations over the increasing sea ice area [*Asplin et al.*, 2009]. Our results are similar in that there are more streak episodes with shorter length (Table 5) in OND than JJA.

3.3. Ice Treatment Differences

[29] An original motivation for this work was to analyze differences in Arctic atmospheric circulation due to differences in sea ice treatment (fractional versus binary). Ultimately, we found no significant differences in atmospheric circulation resulting from sea ice treatment; we document briefly here the basis for arriving at this conclusion.

[30] The largest differences in MSLP between the two ice treatment cases occur in October, although August shows comparable differences in the ABCH seas (Figure 4). However, the maximum differences between the two ice treatment cases in Figure 4 are only about 4 hPa. For comparison, we have computed the August and October interannual variability of monthly MSLP for our domain using the ERA-Interim Re-analysis for 20 years (1989–2008). The standard deviations of the variability for August (3.0 hPa) and October (3.9 hPa) are comparable to the MSLP differences in Figure 4, so the differences are only slightly greater than interannual variability. Using interannual variability as a measure of uncertainty, we find that there are no grid points with differences significant at the 95% level. In addition, a *t* test analysis on a gridpoint-by-gridpoint basis throughout the domain showed no field significance in the differences at the 95% level. Moreover, the monthly mean differences in surface sensible heat flux (Figure 5) are simply a consequence of differences in the direction in which the monthly average winds (not shown) blow for each ice treatment. Like MSLP, differences in surface sensible heat flux are about the same or smaller than their interannual variability (August, 4.3 W–m^2; October, 8.6 W–m^2), so that differences are not significant at the 95% level. A *t* test analysis on a gridpoint-by-gridpoint basis throughout the domain again showed no field significance in the differences at the 95% level. The largest differences are also confined to relatively small areas, suggesting little field significance for the differences. In addition, examination of other fields, such as temperature, winds above the surface and storm tracks (not shown), shows no sign of any thermally forced circulation differences.

[31] Overall, the results suggest that August and October mean MSLP differences in Figure 4 are not the result of changes in ice treatment, but rather a consequence of the ensembles for each ice treatment falling by chance into different monthly average patterns, with no significant forcing differences (e.g., differences in surface sensible heat flux). We note that our work specifies different changes to the lower boundary conditions than previous studies [*Parkinson et al.*, 2001; *Alexander et al.*, 2004; *Deser et al.*, 2004; *Singarayer et al.*, 2006; *Bhatt et al.*, 2008; *Strey et al.*, 2010] and thus does not contradict them. In our work, the distinction is between grid boxes in our target region whose ice cover is typically either 100% (binary) or 50–100% (fractional), in contrast to the cited studies, which explored effects of substantial reductions in overall ice cover.

4. Conclusions and Discussion

[32] In this study, we examined the susceptibility of an Arctic atmospheric-circulation ensemble to developing

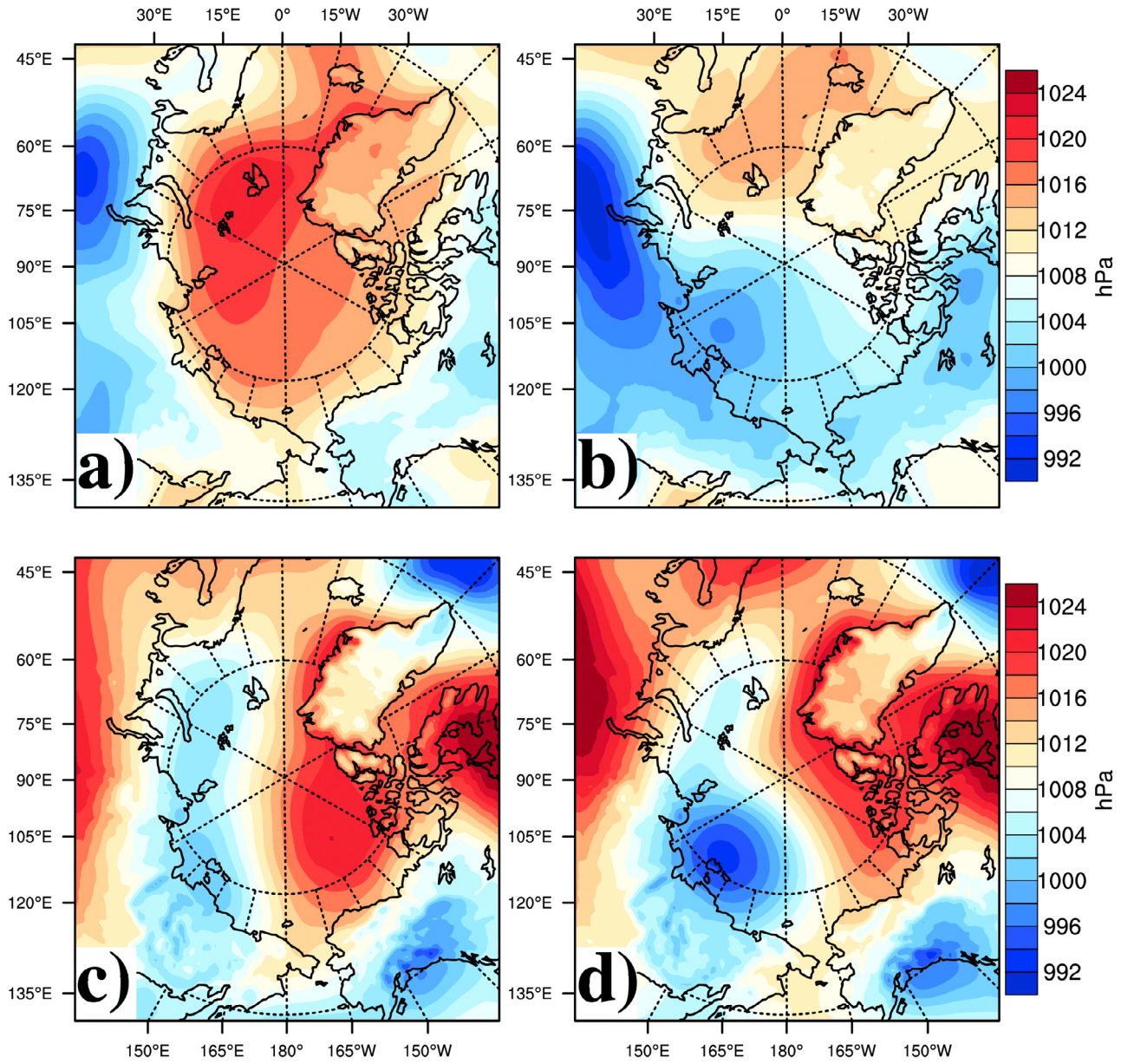

Figure 3. Examples of two regimes corresponding to the cases in Figure 2: (a) high-pressure regimes and (b) low-pressure regimes for the case of two separated regimes; and (c) high-pressure regimes and (d) low-pressure regimes for the case of two regimes with different trends.

multiple dynamic regimes. We used the WRF-ARW model to construct an ensemble containing sixteen members in order to obtain a climate response above noise levels. Initial and boundary conditions were supplied by the ERA-Interim Re-analysis. Our simulations ran from late May 2007 through December 2007 with our period of analysis beginning 15 June, allowing time for the ensemble simulations to spin up and potentially reach distinctly different atmospheric

Table 3. Percentage of Days in Each Month When Two or Three Regimes Are Preferred to One Regime

Month	7 Day	11 Day
June	93%	100%
July	71%	87%
August	84%	97%
September	33%	30%
October	74%	94%
November	63%	83%
December	96%	100%

Table 4. Monthly Averaged Interquartile Differences of the Ensemble's Daily MSLP in the Analysis Region

Month	75th–25th Difference
June (15–30)	6.1
July	4.9
August	8.1
September	5.7
October	10.1
November	9.0
December	9.8

Table 5. Length (in Days) of Streaks When Multiple Regimes Are Preferred With a 7 or 11 Day Window During JJA and OND

Season	Streaks	Average Length
JJA (7 day)	1, 4, 5, 5, 6, 13, 13, 16	7.9
JJA (11 day)	18, 19, 35	24.0
OND (7 day)	1, 1, 1, 3, 4, 6, 7, 8, 8, 9, 18	6.0
OND (11 day)	1, 11, 12, 25, 26	15.0

states by the start of the analysis period. From our simulation output, we constructed daily MSLP time series to analyze for multiple dynamic regimes.

[33] For our regime analysis, we used a Bayesian Information Criterion to determine when multiple regimes persisted for 7 or 11 days. The analysis thus identified multiregime states that persisted beyond synoptic, autoregressive time scales (~5 days). We found that multiple dynamic regimes were common during our simulation period. When sea ice area was declining (JJA) there was a tendency for more persistent multiple-regime behavior, which may be due to sea surface temperatures constraining variability of atmospheric circulation. In contrast, during periods when there was large sea ice area (OND), the interactive ice surface gave the modeled atmosphere more freedom in its variability, potentially allowing less persistent multiple-regime behavior. However, the clearest feature in our simulations occurred in September, when the sea ice area reached a minimum. September had the largest percentage of consecutive days when one-regime behavior was preferred to two-regime or three-regime behavior, possibly due to the constraint on flow evolution posed by the relatively large area with specified sea surface temperatures.

[34] An original intent of this work was to study effects of binary (0% or 100%) sea ice treatment versus fractional sea ice treatment in the model. MSLP differences between fractional and binary sea ice ensembles were largest for October. However, October differences lacked any clear forcing mechanism and were not statistically significant at the 95% level. Only small differences occurred between ensembles in 2 m air temperature, surface sensible heat flux and storm tracks, suggesting the differences between ensembles are not physically meaningful. Longer simulations may be necessary to give a more statistically significant result, although the physical meaningfulness would still be in question, based on our results.

[35] The regime behavior seen here may have implications for the predictability of Arctic atmospheric circulations. Further changes in sea ice area may affect the degree to which multiple persistent regimes appear in ensemble simulations. In the last decade, the Arctic has seen reductions in summer sea ice area [*Serreze et al.*, 2003; *Stroeve et al.*, 2007; *Comiso et al.*, 2008]. The trend may continue in the future [*Zhang and Walsh*, 2006], leading to more one-regime behavior as less sea ice is present. This behavior may allow for more accurate prediction of future Arctic atmospheric circulation in summer because there would be fewer multiregime periods and thus only a single evolution path for atmospheric circulation.

[36] Limitations on model variability exist due to our use of specified sea surface temperatures, which prevent interactive changes in ocean temperature. This limitation would be more common during periods of low sea ice, i.e., late summer. Using a coupled ocean-atmosphere model may produce more multiple-regime states during low ice periods than our specified sea surface temperature simulations

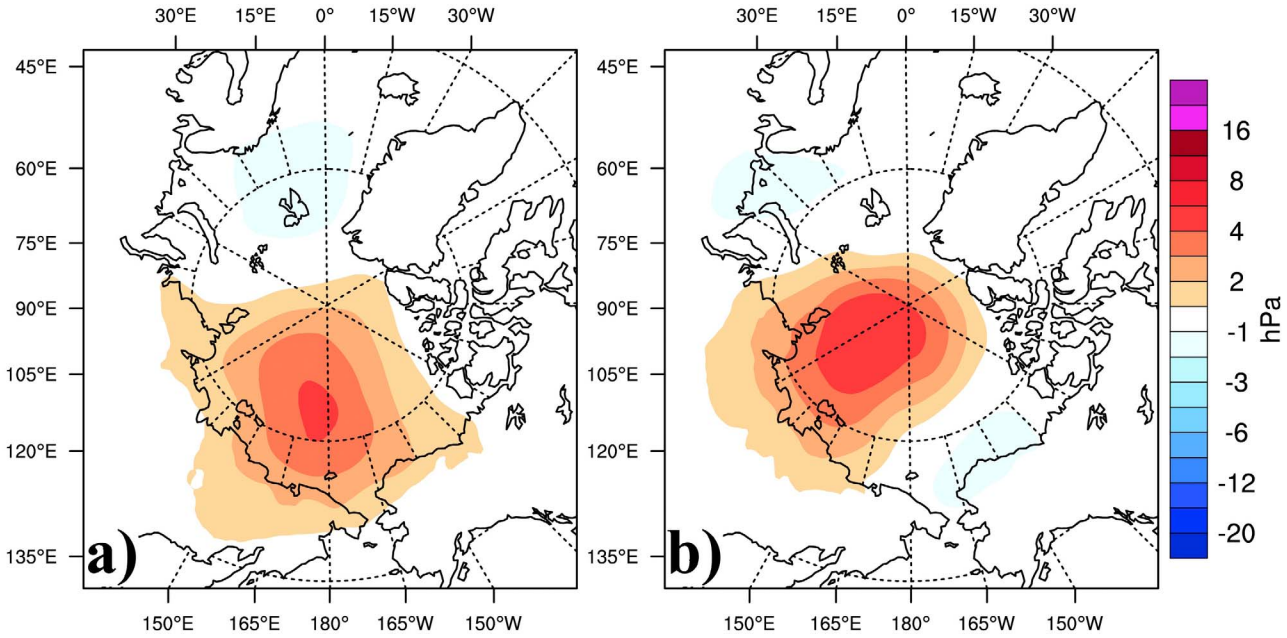

Figure 4. Monthly averaged MSLP differences for fractional-binary ensembles for (a) August and (b) October. Note that the contour interval increases with increasingly larger magnitude of differences. The scales are the same for positive and negative differences.

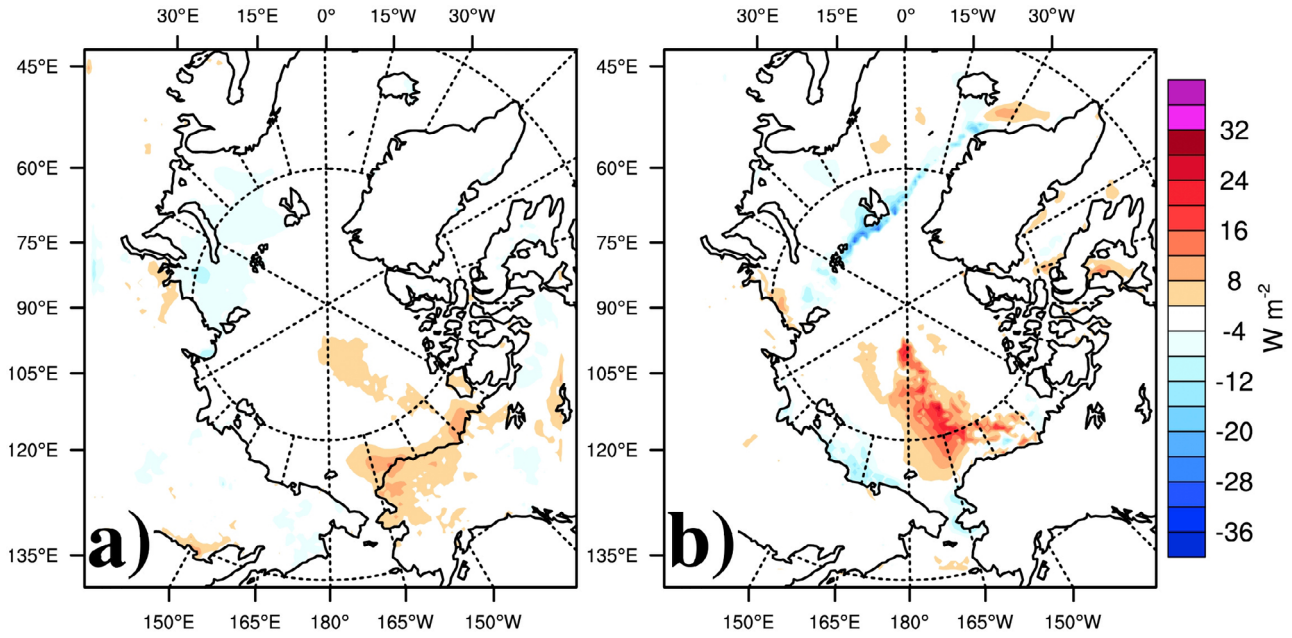

Figure 5. Fractional-binary ensemble differences for monthly averaged sensible heat flux differences for (a) August and (b) October.

because there would be more interaction between the ocean and atmosphere. However, ocean temperatures tend to evolve more slowly than ice surface temperatures, which may lessen the effects of an interactive ocean.

[37] **Acknowledgments.** This work was supported by U.S. Department of Energy grant DE-A102-98ER62596. The data for this study are from the Research Data Archive (RDA), which is maintained by the Computational and Information Systems (CIS) laboratory at the National Center for Atmospheric Research (NCAR). NCAR is sponsored by the National Science Foundation (NSF). The original data are available from the RDA (http://dss.ucar.edu) in data set ds627.0. Computer support was provided by the University of Alaska Arctic Region Supercomputing Center (ARSC) and NCAR Command Language (NCL) online reference manual.

References

Alexander, M. A., U. S. Bhatt, J. E. Walsh, M. S. Timlin, J. S. Miller, and J. D. Scott (2004), The atmospheric response to realistic Arctic sea ice anomalies in an AGCM during winter, *J. Clim.*, *17*, 890–905.

Alexandru, A., R. de Elia, and R. Laprise (2007), Internal variability in regional climate downscaling at the seasonal scale, *Mon. Weather Rev.*, *135*, 3221–3238, doi:10.1175/MWR3456.1.

Asplin, M. G., J. V. Lukovich, and D. G. Barber (2009), Atmospheric forcing of the Beaufort Sea ice gyre: Surface pressure climatology and sea ice motion, *J. Geophys. Res.*, *114*, C00A06, doi:10.1029/2008JC005127.

Berrisford, P., D. Dee, K. Fielding, M. Fuentes, P. Kallberg, S. Kobayashi, and S. Uppala (2009), The ERA-Interim Archive, *ERA Rep. Ser. 1*, 16 pp., Eur. Cent. for Medium-Range Weather Forecasts, Reading, U. K.

Bhatt, U. S., M. A. Alexander, C. Deser, J. E. Walsh, J. S. Miller, M. S. Timlin, J. Scott, and R. A. Tomas (2008), The atmospheric response to realistic reduced summer Arctic sea ice anomalies, in *Arctic Sea Ice Decline: Observations, Projections, Mechanisms, and Implications*, *Geophys. Monogr. Ser.*, vol. 180, edited by E. T. DeWeaver et al., pp. 91–110, AGU, Washington, D. C.

Cassano, J. J., M. E. Higgins, and M. W. Seefeldt (2011), Performance of the weather research and forecasting (WRF) model for month-long Pan-Arctic simulations, *Mon. Weather Rev.*, doi:10.1175/MWR-D-10-05065.1, in press.

Charney, J. G., and J. G. DeVore (1979), Multiple flow equilibria in the atmosphere and blocking, *J. Atmos. Sci.*, *36*, 1205–1216.

Chen, F., and J. Dudhia (2001), Coupling an advanced land surface–hydrology model with the Penn State–NCAR MM5 modeling system. Part I: Model implementation and sensitivity, *Mon. Weather Rev.*, *129*, 569–585.

Collins, W. D., et al. (2004), Description of the NCAR Community Atmosphere Model (CAM 3.0), *Tech. Rep. NCAR/TN-464+STR*, 171 pp., Natl. Cent. for Atmos. Res., Boulder, Colo.

Comiso, J. C. (2006), Abrupt decline in the Arctic winter sea ice cover, *Geophys. Res. Lett.*, *33*, L18504, doi:10.1029/2006GL027341.

Comiso, J. C. (2008), Bootstrap Sea Ice Concentrations for NIMBUS-7 SSMR and DMSP SSM/I, http://nsidc.org/data/nsidc-0079.html, Natl. Snow and Ice Data Cent., Boulder, Colo.

Comiso, J. C., and R. Kwok (1996), Surface and radiative characteristics of the summer Arctic sea ice cover from multisensor satellite observations, *J. Geophys. Res.*, *101*(C12), 28,397–28,416, doi:10.1029/96JC02816.

Comiso, J. C., and C. L. Parkinson (2008), Arctic sea ice parameters from AMSR-E data using two techniques and comparisons with sea ice from SSM/I, *J. Geophys. Res.*, *113*, C02S05, doi:10.1029/2007JC004255.

Comiso, J. C., D. J. Cavalieri, C. L. Parkinson, and P. Gloersen (1997), Passive microwave algorithms for sea ice concentrations: A comparison of two techniques, *Remote Sens. Environ.*, *60*, 357–384.

Comiso, J. C., C. L. Parkinson, R. Gersten, and L. Stock (2008), Accelerated decline in the Arctic sea ice cover, *Geophys. Res. Lett.*, *35*, L01703, doi:10.1029/2007GL031972.

Deser, C., G. Magnusdottir, R. Saravanan, and A. Phillips (2004), The effects of North Atlantic SST and sea ice anomalies on the winter circulation in CCM3, Part II: Direct and indirect components of the response, *J. Clim.*, *17*, 877–889.

Fraley, C., and A. E. Raftery (2002), Model-based clustering, discriminant analysis, and density estimation, *J. Am. Stat. Assoc.*, *97*, 611–631.

Francis, J. A., W. Chan, D. Leathers, J. R. Miller, and D. E. Veron (2009), Winter Northern Hemisphere weather patterns remember summer Arctic sea ice extent, *Geophys. Res. Lett.*, *36*, L07503, doi:10.1029/2009GL037274.

Giorgi, F., and X. Bi (2000), A study of internal variability of a regional climate model, *J. Geophys. Res.*, *105*(D24), 25,503–29,521, doi:10.1029/2000JD900269.

Grell, G. A., and D. Devenyi (2002), A generalized approach to parameterizing convection combining ensemble and data assimilation techniques, *Geophys. Res. Lett.*, *29*(14), 1693, doi:10.1029/2002GL015311.

Gutowski, W. J., Jr., H. Wei, C. J. Vörösmarty, and B. M. Fekete (2007), Influence of Arctic wetlands on Arctic atmospheric circulation, *J. Clim.*, *20*, doi:10.1175/JCLI4243.1.

Hansen, A. R. (1988), Further observational characteristics of bimodal planetary waves: Mean structure and transitions, *Mon. Weather Rev.*, *116*, 386–400.

Higgins, M. E., and J. J. Cassano (2009), Impacts of reduced sea ice on winter Arctic atmospheric circulation, precipitation, and temperature, *J. Geophys. Res.*, *114*, D16107, doi:10.1029/2009JD011884.

Hines, K. M., D. H. Bromwich, L.-S. Bai, M. Barlage, and A. G. Slater (2011), Development and testing of Polar WRF, Part III: Arctic land, *J. Clim.*, *24*, doi:10.1175/2010JCLI3460.1.

Honda, M., K. Yamazaki, Y. Tachibana, and K. Takeuchi (1996), Influence of Okhotsk sea ice extent on atmospheric circulation, *Geophys. Res. Lett.*, *23*(24), 3595–3598, doi:10.1029/1996GL03474.

Janjic, Z. I. (2001), Nonsingular implementation of the Mellor-Yamada Level 2.5 scheme in the NCEP Meso model, *NCEP Off. Note 437*, 61 pp., NOAA Sci. Cent., Camp Springs, Md.

Lucas-Picher, P., D. Caya, S. Biner, and R. Laprise (2008), Investigation of regional climate models' internal variability with a ten-member ensemble of 10-year simulations over a large domain, *Clim. Dyn.*, *31*, 927–940, doi:10.1007/s00382–008–0384–8.

Mlawer, E. J., S. J. Taubman, P. D. Brown, M. J. Iacono, and S. A. Clough (1997), Radiative transfer for inhomogeneous atmospheres: RRTM, a validated correlated-k model for the longwave, *J. Geophys. Res.*, *102*(D14), 16,663–16,682, doi:10.1029/97JD00237.

Monin, A. S., and A. M. Obukhov (1954), Basic laws of turbulent mixing in the surface layer of the atmosphere, *Contrib. Geophys. Inst. Acad. Sci. USSR*, *151*, 163–187.

Parkinson, C. L., D. Rind, R. J. Healy, and D. G. Martinson (2001), The impact of sea ice concentration accuracies on climate model simulations with the GISS GCM, *J. Clim.*, *14*, 2606–2623.

Petoukhov, V., and V. A. Semenov (2010), A link between reduced Barents-Kara sea ice and cold winter extremes over northern continents, *J. Geophys. Res.*, *115*, D21111, doi:10.1029/2009JD013568.

Raftery, A. E., T. Gneiting, F. Balabdaoui, and M. Plakowski (2005), Using Bayesian model averaging to calibrate forecast ensembles, *Mon. Weather Rev.*, *133*, 1155–1174.

Rinke, A., and K. Dethloff (2000), On the sensitivity of a regional Arctic climate model to initial and boundary conditions, *Clim. Res.*, *14*, 101–113.

Rutledge, S. A., and P. V. Hobbs (1984), The mesoscale and microscale structure and organization of clouds and precipitation in midlatitude cyclones, Part XII: A diagnostic modeling study of precipitation development in narrow cloud-frontal rainbands, *J. Atmos. Sci.*, *20*, 2949–2972.

Serreze, M. C., J. A. Maslanik, T. A. Scambos, F. Fetterer, J. Stroeve, K. Knowles, C. Fowler, S. Drobot, R. G. Barry, and T. M. Haran (2003), A record minimum Arctic sea ice extent and area in 2002, *Geophys. Res. Lett.*, *30*(3), 1110, doi:10.1029/2002GL016406.

Serreze, M. C., M. M. Holland, and J. Stroeve (2007), Perspectives on the Arctic's shrinking sea ice cover, *Science*, *315*, 1533–1536.

Simmons, A., S. Uppala, D. Dee, and S. Kobayahsi (2007), ERA-Interim: New ECMWF reanalysis products from 1989 onwards, *ECMWF Newsl.*, 110, pp. 25–35, Eur. Cent. for Medium-Range Weather Forecasts, Reading, U. K.

Singarayer, J. S., J. L. Bamber, and P. J. Valdes (2006), Twenty-first-century climate impacts from a declining Arctic sea ice cover, *J. Clim.*, *19*, 1109–1125.

Sivillo, J. K., J. E. Ahlquist, and Z. Toth (1997), An ensemble forecasting primer, *Weather Forecasting*, *12*, 809–818.

Skamarock, W. C., J. B. Klemp, J. Dudhia, D. O. Gill, D. M. Barker, M. G. Duda, X.-Y. Huang, W. Wang, and J. G. Powers (2008), A description of the advanced research WRF version 3, *Tech. Note NCAR/TN-475+STR*, 113 pp., Natl. Cent. for Atmos. Res., Boulder, Colo.

Slonosky, V. C., L. A. Mysak, and J. Derome (1997), Linking Arctic sea ice and atmospheric circulation anomalies on interannual and decadal timescales, *Atmos. Ocean*, *35*, 333–366.

Smyth, P., K. Ide, and M. Ghil (1999), Multiple regimes in Northern Hemisphere height fields via mixture model clustering, *J. Atmos. Sci.*, *56*, 3704–3723.

Sorteberg, A., and J. E. Walsh (2008), Seasonal cyclone variability at 70°N and its impact on moisture transport into the Arctic, *Tellus, Ser. A*, *60*, 570–586, doi:10.1111/j.1600–0870.2008.00314.x.

Strey, S. T., W. L. Chapman, and J. E. Walsh (2010), The 2007 sea ice minimum: Impacts on the Northern Hemisphere atmosphere in late autumn and early winter, *J. Geophys. Res.*, *115*, D23103, doi:10.1029/2009JD013294.

Stroeve, J., M. M. Holland, W. Meier, T. Scambos, and M. Serreze (2007), Arctic sea ice decline: Faster than forecast, *Geophys. Res. Lett.*, *34*, L09501, doi:10.1029/2007GL029703.

Tao, W.-K., and J. Simpson (1993), The Goddard cumulus ensemble model, Part I: Model description, *Terr. Atmos. Oceanic Sci.*, *4*, 19–54.

Taschetto, A. S., and M. H. England (2008), Estimating ensemble size requirements of AGCM simulations, *Meteorol. Atmos. Phys.*, *100*, 23–26, doi:10.1007/s00703–008–0293–8.

Walsh, J. E. (1983), The role of sea ice in climatic variability: Theories and evidence, *Atmos. Ocean*, *21*, 229–242.

Walsh, J. E., and C. M. Johnson (1979), An analysis of Arctic sea ice fluctuations, 1953–77, *J. Phys. Oceanogr.*, *9*, 580–591.

Wu, W., A. H. Lynch, and A. Rivers (2005), Estimating the uncertainty in a regional climate model related to initial and lateral boundary conditions, *J. Clim.*, *18*, 917–933.

Zhang, X., and J. E. Walsh (2006), Toward a seasonally ice-covered Arctic Ocean: Scenarios from the IPCC AR4 model simulations, *J. Clim.*, *19*, 1730–1747.

Zhang, X., J. E. Walsh, J. Zhang, U. S. Bhatt, and M. Ikeda (2004), Climatology and interannual variability of Arctic cyclone activity: 1948–2002, *J. Clim.*, *17*, 2300–2317.

J. J. Cassano, Department of Atmospheric and Oceanic Sciences, University of Colorado at Boulder, Box 216 UCB, Boulder, CO 80309, USA. (john.cassano@colorado.edu)

B. J. Fisel, W. J. Gutowski Jr., and J. M. Hobbs, Department of Geological and Atmospheric Sciences, Iowa State University, 3021 Agronomy Hall, Ames, IA 50011, USA. (bjfisel@iastate.edu; gutowski@iastate.edu; jonhobbs@iastate.edu)